III. PHYSICAL ELECTRONICS AND SURFACE PHYSICS[*]

Academic and Research Staff

Prof. R. E. Stickney
Dr. A. E. Dabiri

Graduate Students

P. C. Abbott	T. L. Bradley	C. N. Lu
V. S. Aramati	T. E. Kenney	D. V. Tendulkar

A. DIFFRACTION OF HELIUM ATOMS FROM A TUNGSTEN (112) CRYSTAL SURFACE[*]

1. Introduction

During the last forty years there have been numerous investigations of the diffraction of atoms and molecules from solid surfaces. Early in the 1930's, Stern, Estermann, and Frisch[1] observed the diffraction of thermal beams of He and H_2 from LiF and NaCl single crystals. Many workers[2] have reconfirmed and extended these results for alkali halide crystals, but no one has reported observing either atomic or molecular diffraction from a metal crystal. There have been numerous studies of the scattering of He, H_2, and D_2 from various metal crystals,[3-9] and the general finding is a lobular scattering pattern peaked at the specular angle with no indication of secondary peaks corresponding to diffraction of order greater than zero. Recently, Weinberg and Merrill[10] have observed the diffraction of helium and deuterium beams from a tungsten carbide surface structure on a W(110) crystal, but the diffraction effects disappeared when the carbon was removed. We report here the diffraction of helium from a W(112) crystal that is believed to be clean. This is the first instance of atomic diffraction from a pure (i. e. , clean) metal surface.

2. Experimental Apparatus

The experimental apparatus is identical to that described elsewhere,[5] except that the target chamber is now pumped by an ion pump and the detector is a stagnation-type ionization gauge. The target chamber pressure is of the order of 1×10^{-9} Torr after baking at 200°C. A nearly monoenergetic molecular beam, generated by a nozzle source, strikes the target that is situated at the center of the target chamber. Detection of either the incident beam or the scattered beam in the principal scattering plane is accomplished by the rotatable detector.

The tungsten target is a disc, 0.6 cm in diameter, oriented and spark-cut from a high-purity single crystal so that the surface is the (112) face. Before mounting, the crystal surface was polished, first mechanically and then electrolytically, and the orientation was checked by the Laue x-ray diffraction technique. After installing the crystal in the apparatus and baking the system during evacuation, the surface was cleaned. Specifically, the carbon impurities were removed by the oxidation procedure described by Germer and May,[11] that is, a repeated cycle of heating the crystal at ~1300°K in ~2 × 10^{-7} Torr O_2 for a considerable time and then flashing for a few seconds above 2400°K. (Our confidence in this procedure is strengthened by the fact that no impurities were detectable by Auger electron spectroscopy when a similar crystal was cleaned in this manner in an auxiliary apparatus.) Before measuring a scattering pattern, the crystal was flashed (i.e., heated to ~2400°K for several seconds by electron bombardment) to remove adsorbable background gases. Unfortunately, the background pressure (~1 × 10^{-9} Torr with beam off) proved to be too high to keep the surface clean for the length of time required to measure a scattering pattern unless T_s > 1200°K. Hence we could not obtain reliable scattering patterns for T_s below ~1300°K (see Yamamoto and Stickney[5] for detailed discussion of this point).

The (112) face of a tungsten crystal has a highly anisotropic surface structure, comprising closely packed rows of top-layer atoms in the $[11\bar{1}]$ azimuthal direction, separated by relatively open channels or "troughs" as shown in Fig. III-1. By comparing
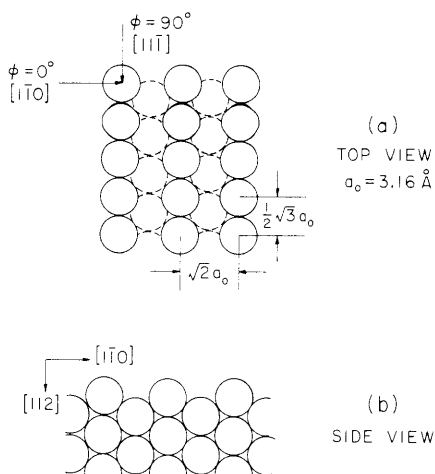

Fig. III-1.   Atomic structure of the (112) face of a tungsten single crystal.

the scattering patterns for two azimuthal directions (ϕ = 0° and ϕ = 90° in Fig. III-1), we hoped to determine the sensitivity of atom-solid collisions to the atomic structure of the surface. The diffraction-grating spacing in the principal scattering plane is d = 4.47 Å in the ϕ = 0° $[1\bar{1}0]$ direction and d = 2.74 Å in the ϕ = 90° $[11\bar{1}]$ direction.

The temperature of the beam gas was the same, ~300°K, for all experimental runs. For an ideal nozzle beam, the helium beam would be nearly monoenergetic with speed approximately equal to 1.76×10^5 cm/s for a source temperature of ~300°K. (The nozzle beams have been described by others.[12,13]) Therefore, the corresponding de Broglie wavelength, λ, would be 0.565 Å. The expected angular position, θ_{rn}, of the nth-order diffracted beam may be obtained from the simple diffraction relation

$$\sin \theta_{rn} - \sin \theta_i = \frac{n\lambda_i}{d}, \tag{1}$$

where θ_i is the angle of incidence, and d is the diffraction-grating spacing.

The flux and halfwidth (i.e., the full width at half-maximum) of the incident beam are measured with the detector by lifting the crystal out of the beam. The measured peak flux of the beam, F_o, is used to normalize the scattered flux, F_s. The measured halfwidth of the beam is ~5° in terms of the angular rotation of the detector. Since the acceptance angle of the detector is ~4°, the true halfwidth of the beam is substantially less than the measured value. (We estimate from our measurements that the true halfwidth is ~2.8°.)

3. Experimental Results

Figure III-2 shows the He scattering patterns for $\phi = 0°$ $[1\bar{1}0]$ when the crystal temperature, T_s, is ~1300°K. The scattering patterns for $\theta_i = 30°$ and 40° exhibit three peaks, whereas only two peaks are observed for $\theta_i = 50°$ and 60°. Notice that the angular positions of these peaks agree very closely with the theoretical predictions (indicated by arrows in Fig. III-2) obtained from Eq. 1 for the (00), (10), and ($\bar{1}$0) diffraction peaks.

The intensity of the specular or (00) peak is observed to increase significantly with increase in the angle of incidence, θ_i. Specifically, $(F_s/F_o)_{spec}$ increases from 0.047 for $\theta_i = 30°$ to 0.24 for $\theta_i = 60°$. Note that the individual peaks become increasingly narrow with increasing angle of incidence. The halfwidth of the specular peak at $\theta_i = 60°$ is ~6°, which corresponds closely to the measured halfwidth of the incident beam (~5°, as described above).

Figure III-3 shows the scattering patterns for $\phi = 0°$ $[1\bar{1}0]$ with $T_s = 2200°K$ and $\theta_i = 45°$ and 60°. The patterns are broader than those for $T_s \approx 1300°K$ (Fig. III-2), and only the specular peak is observed. By comparing the data for $\theta_i = 60°$ in Figs. III-2 and III-3, we see that the intensity of the peak decreases by a factor of three when T_s is increased from 1300°K to 2200°K. This decrease in peak intensity with increasing T_s is consistent with the results obtained by other investigators.[6-8] One of the possible reasons for the increased broadening and decreased intensity at higher temperatures is that the perfection of the surface structure (the diffraction grating)
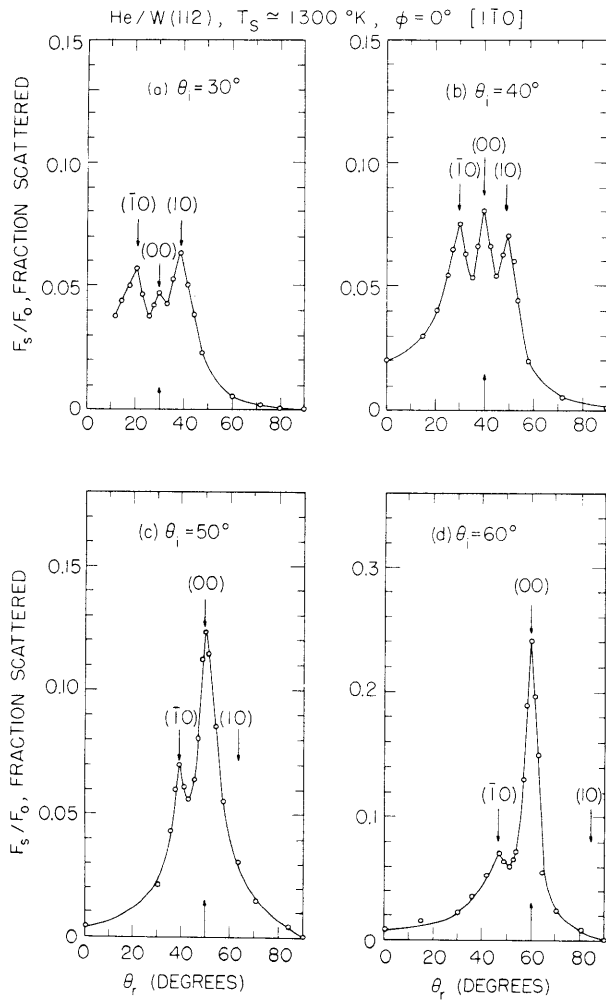
Fig. III-2.

Scattering patterns for helium scattered from a W(112) crystal. Beam conditions: $\phi = 0°$ $[1\bar{1}0]$, $\theta_i = 30°$, $40°$, $50°$, and $60°$, $T_b = 300°$K. Target conditions: $T_s \approx 1300°$K. Arrows indicate the positions of the diffraction peaks predicted by simple diffraction theory.

Fig. III-3.
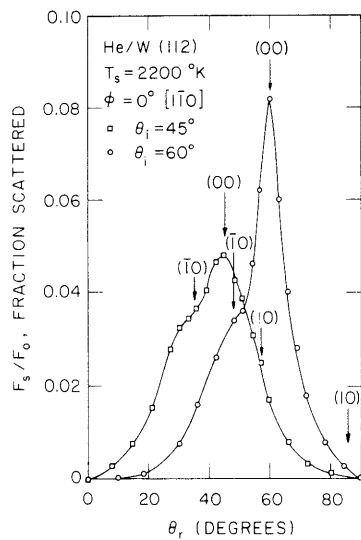
Scattering patterns for helium scattered from a W(112) crystal. Beam conditions: $\phi = 0°$ $[1\bar{1}0]$, $\theta_i = 45°$ and $60°$, $T_b = 300°$K. Target conditions: $T_s \approx 2200°$K.

is degraded by thermal motion, as observed in low-energy electron diffraction studies.[14] Data were obtained at various values of T_s, and we found that the (10) and ($\bar{1}$0) peaks could be resolved only for $T_s \lesssim 1900°$K.

The scattering patterns for $\phi = 90°$ [11$\bar{1}$] with $T_s \approx 1300°$K and $\theta_i = 45°$ and $60°$ are shown in Fig. III-4a. In this case, there are no distinguishable peaks other than the (00) specular peak. (The arrows in Fig. III-4 indicate the predicted positions of the first-order diffraction peaks.) Note that the intensity of the specular peak is much smaller
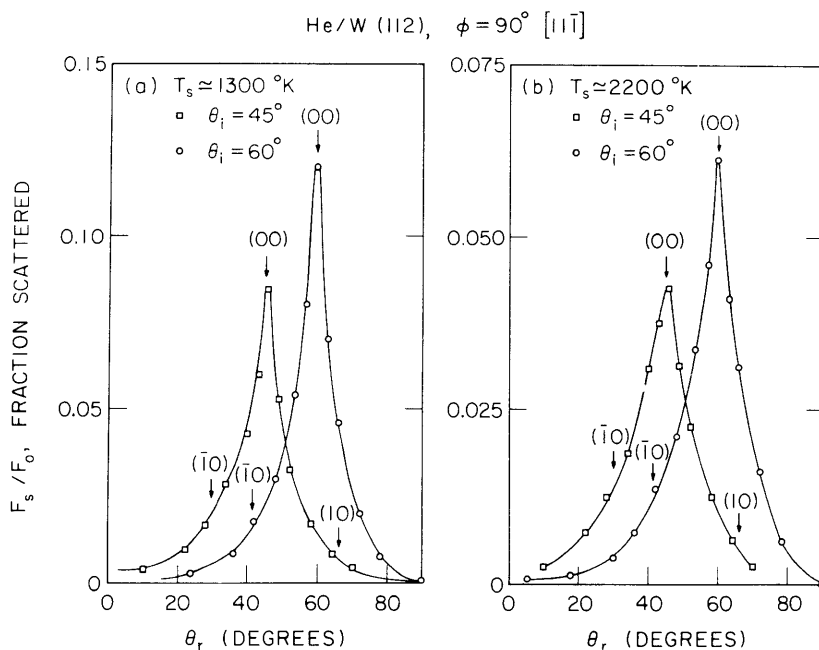

He/W (112), $\phi = 90°$ [11$\bar{1}$]

Fig. III-4. Scattering patterns for helium scattered from a W(112) crystal.
Beam conditions: $\phi = 90°$ [11$\bar{1}$], $\theta_i = 45°$ and $60°$, $T_b = 300°$K.
Target conditions: $T_s \approx 1300°$ and $2200°$K.

in this case than for $\phi = 0°$ [1$\bar{1}$0]. For example, the peak intensity for $\theta_i = 60°$ and $T_s \approx 1300°$K is roughly a factor of two less for $\phi = 90°$ [11$\bar{1}$] than for $\phi = 0°$ [1$\bar{1}$0].

The corresponding data for $T_s = 2200°$K are shown in Fig. III-4b. The general shape of the patterns is similar to that for $T_s \approx 1300°$K, but the intensities are smaller and the halfwidths are larger, as observed for $\phi = 0°$ [1$\bar{1}$0].

4. Conclusion

The most interesting aspect of the present results is that atomic diffraction has been observed from a metal surface which we believe to be clean. As can be seen in Fig. III-2, the peaks for $\phi = 0°$ [1$\bar{1}$0] are sharp and well resolved, and their angular positions agree

well with the predicted positions of the (00), (10), and ($\bar{1}$0) diffraction peaks. The data for ϕ = 90° [11$\bar{1}$] in Fig. III-4, however, do not exhibit peaks other than the (00) specular peak. It seems reasonable to suspect that this dependence on azimuthal direction arises because the surface structure is far more pronounced (atomically "rough" or non-planar) in the [1$\bar{1}$0] direction than in the [11$\bar{1}$] direction. This would cause the periodic variation of the interaction potential "seen" by the incident He atoms to be significantly stronger for ϕ = 0° [1$\bar{1}$0] than for ϕ = 90° [11$\bar{1}$]. Existing theoretical treatments of atom-solid diffraction predict that the intensity of the first-order peaks should increase with the strength of the periodic interaction potential.[15] Since the crystal orientations employed in previous experimental investigations of the scattering of He from metals[3-9,16] have less pronounced ("smoother") atomic surface structures than W(112), we suspect that the periodic variations of the interaction potentials were so small that the first-order diffraction peaks were either below the level of detection or completely masked by inelastically scattered atoms.

<div align="right">D. V. Tendulkar, R. E. Stickney</div>

References

1. I. Estermann and O. Stern, Z. Physik 61, 195 (1930) and 73, 348 (1931); R. Frisch and O. Stern, Z. Physik 84, 430 (1933); R. Frisch, Z. Physik 84, 443 (1933).

2. For example, see the references listed in D. R. O'Keefe, J. N. Smith, Jr., R. L. Palmer, and H. Saltsburg, J. Chem. Phys. 52, 4447 (1970).

3. J. N. Smith, Jr., and H. Saltsburg, in H. Saltsburg, J. N. Smith, Jr., and M. Rogers (Eds.), Fundamentals of Gas-Surface Interactions (Academic Press, Inc., New York, 1967), p. 370.

4. J. N. Smith, Jr., H. Saltsburg, and R. L. Palmer, in L. Trilling and H. Y. Wachman (Eds.), Rarefied Gas Dynamics, Proc. 6th International Symposium, Vol. 2 (Academic Press, Inc., New York, 1969), pp. 1141-1157.

5. S. Yamamoto and R. E. Stickney, J. Chem. Phys. 53, 1594 (1970).

6. D. L. Smith and R. P. Merrill, J. Chem. Phys. 53, 3558 (1970).

7. A. G. Stoll, D. L. Smith, and R. P. Merrill, J. Chem. Phys. 54, 163 (1971).

8. R. L. Palmer, D. R. O'Keefe, H. Saltsburg, and J. N. Smith, Jr., J. Vac. Sci. Technol. 7, 90 (1970).

9. L. A. West, E. I. Kozak, and G. A. Somorjai, J. Vac. Sci. Technol. 8, 430 (1971).

10. W. H. Weinberg and R. P. Merrill, Phys. Rev. Letters 25, 1198 (1970).

11. L. H. Germer and J. W. May, Surface Sci. 4, 452 (1966).

12. J. B. Anderson, R. P. Andres, and J. B. Fenn, in J. Ross (Ed.), Molecular Beams, Advances in Chemical Physics, Vol. 10 (Interscience Publishers, New York, 1966), pp. 275-317.

13. J. P. Moran, AIAA J. 8, 539 (1970).

14. A. U. MacRae and L. H. Germer, Phys. Rev. Letters 8, 489 (1962); A. U. MacRae, Surface Sci. 2, 522 (1964); E. R. Jones, J. T. McKinney, and M. B. Webb, Phys. Rev. 151, 476 (1966).

15. N. Cabrera, V. Celli, F. O. Goodman, and R. Manson, Surface Sci. 19, 67 (1970); F. O. Goodman, Surface Sci. 19, 93 (1970).

16. The crystal surfaces generally were either FCC(111) or BCC(110), which are the smoothest possible surfaces.

B. EXPERIMENTAL MEASUREMENTS OF THE SPEED DISTRIBUTIONS OF DEUTERIUM MOLECULES DESORBED FROM NICKEL SURFACES

1. Introduction

This study is a continuation of our previous experimental investigations of the spatial and speed distributions of hydrogenic molecules (H_2, D_2, HD) desorbed from polycrystalline and single-crystal nickel surfaces.[1,2] We have discovered that the time-of-flight curves reported previously[2] are erroneous, because of distortion of the signal by the preamplifier in our detection electronics. These experiments have been repeated and we report here the new data obtained for D_2 desorbed from poly-crystalline and single-crystal (110) nickel surfaces. We also describe a quantitative method for characterizing the data by taking low-order moments of the time-of-flight curves.

2. Moment Method for Characterizing Time-of-Flight Data

In the following description of the moment method for characterizing the time-of-flight (TOF) curves, we shall refer to the time-of-flight experiment shown schematically in Fig. III-5. After molecules in free molecular flow leave the source (which could be a Knudsen cell or a surface from which the molecules desorb), they are chopped at regular intervals by the mechanical chopper. At the end of the flight path, ℓ, some of these molecules are ionized by electron impact. If the time that the chopper is open, t_{co}, is much less than the average flight time, the shape of the chopper opening (the shutter function) may be considered to be a delta function. In this case, the instantaneous number density of particles in the detector is related to the velocity distribution by[3]

$$n(t_i) = K_1 f(v) \frac{\ell^3}{t_i^4},\tag{1}$$

where t_i is the time measured from the instant the chopper opens, $f(v)$ is the velocity distribution, v is the velocity ($v = \ell/t_i$), and K_1 is a constant. A plot of $n(t_i)$ against t_i is called a "TOF" curve.
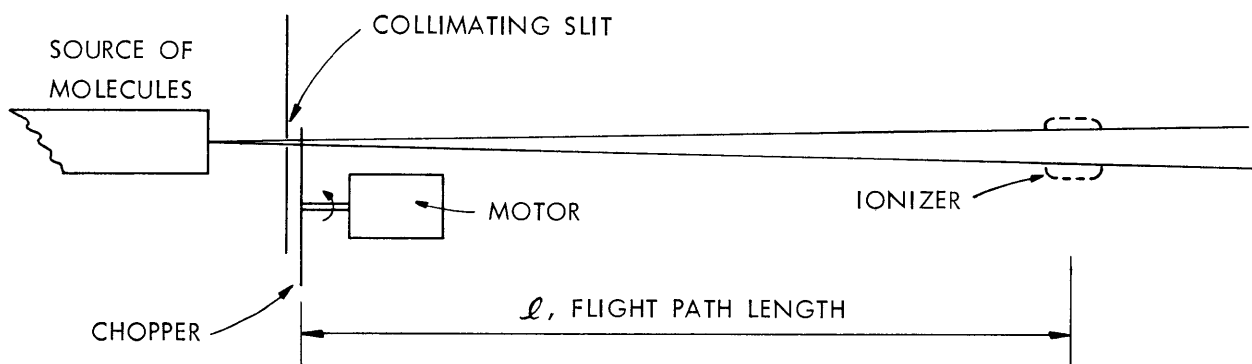
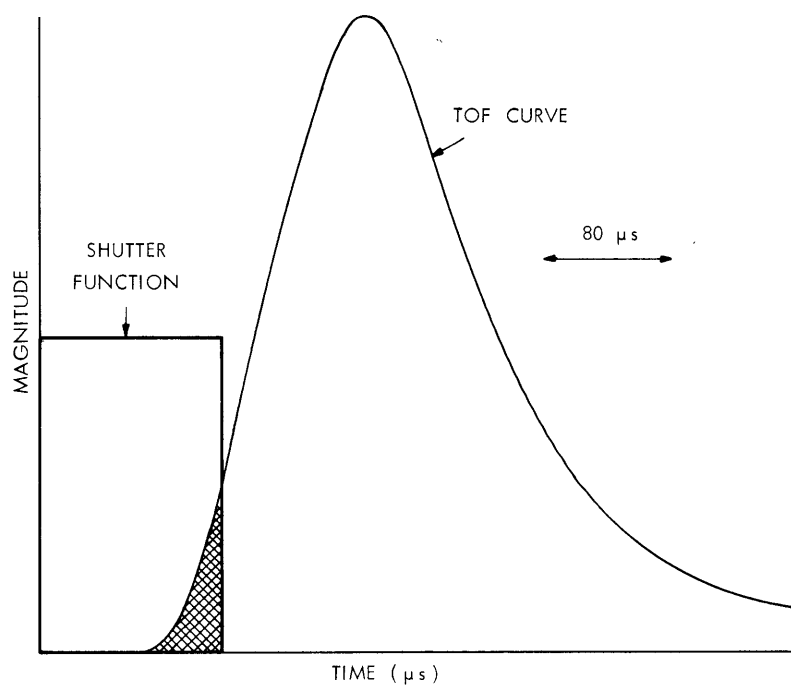Fig. III-5. Simple time-of-flight (TOF) experiment.

Fig. III-6. Time-of-flight curve measured by the apparatus in Fig. III-5 when the shutter function is rectangular. (The crosshatched area represents molecules that have been detected while the chopper is still open.)

If the source in Fig. III-5 is considered to be a slit and the shutter function is rectangular, the TOF distribution measured by the detector would be that shown in Fig. III-6. The crosshatched area in Fig. III-6 represents molecules that have been detected while the chopper is still open. Because t_{co} is of the same order as the average flight time, the TOF curve is affected by the shape and duration of the shutter function. Therefore, the particle number density in the detector is related to the velocity distribution by a convolution integral over the shutter function[3]

$$n(t_i) = K_2 \int_0^{t^*} A(t_c) \, f\left(\frac{\ell}{\tau}\right) \frac{\ell^3}{\tau^4} \, dt_c, \tag{2}$$

where t_c is the time scale for the shutter function, $t^* = t_i$ for $t_i < t_{co}$ and $t^* = t_{co}$ for $t_i > t_{co}$, $\tau = t_i - t_c$, $v = \ell/\tau$, and $A(t_c)$ is the shutter function. To solve Eq. 2 for the velocity distribution, $f\left(\frac{\ell}{\tau}\right) = f(v)$, we shall take the Laplace transform of the equation. The Laplace transform of the right-hand side may be written as the product of two transforms,

$$N(s) = F(s) \, H(s), \tag{3}$$

where

$$N(s) = \mathscr{L}(n(t_i)) \tag{4a}$$

$$F(s) = \mathscr{L}(A(t_c)) \tag{4b}$$

$$H(s) = \mathscr{L}(f(v) \, \ell^3/\tau^4), \tag{4c}$$

and the constant K_2 has been dropped. The velocity distribution is obtained by taking the inverse transform of Eq. 3 and rearranging the terms:

$$f(v) = \frac{\ell}{v^4} \, \mathscr{L}^{-1}(N(s)/F(s)), \tag{5}$$

where $\ell^3/\tau^4 = v^4/\ell$. For our experiments, the shutter function is actually trapezoidal, but it can be approximated accurately by a rectangular shutter function of duration $t_{co} = 116 \pm 4 \, \mu s$. The Laplace transform for a rectangular shutter function $[A(t_c) = A_o$ for $0 \le t_c \le t_{co}; \, A(t_c) = 0$ for $t_c > t_{co}]$ is

$$F(s) = \int_0^{t_{co}} A_o \, e^{-st_c} \, dt_c = \frac{A_o}{s} \left(1 - e^{-st_{co}}\right), \tag{6}$$

where A_o is the height of the shutter function. The reciprocal of F(s) is

$$[F(s)]^{-1} = \frac{s}{A_o} \frac{1}{1 - e^{-st_{co}}} = \frac{s}{A_o} \sum_{r=0}^{\infty} e^{-rst_{co}} \tag{7}$$

Substitution of Eq. 7 in Eq. 5 yields

$$f(v) = \frac{\ell^4}{v^4} \frac{1}{\ell^3} \mathscr{L}^{-1} \left[N(s) \frac{s}{A_o} \sum_{r=0}^{\infty} e^{-rst_{co}} \right]. \tag{8}$$

By letting $\eta = \ell/v$ and taking the inverse Laplace transform of the right side,[4] the velocity distribution is obtained:

$$f(v) = \ell^{-3}\eta^4 \sum_{r=0}^{\infty} \frac{d}{d\eta} n(\eta - rt_{co}), \tag{9}$$

where the constant A_o has been dropped, and $n(\eta - rt_{co})$ is the height of the TOF curve at time $t_i = \eta - rt_{co}$.

A serious drawback of Eq. 9 is that the first derivative of the TOF curve must be evaluated at each t_i. This means that the TOF curve would have to be known very accurately to obtain moderate accuracy in the velocity distribution, f(v). Other investigators[3] have found that it is more appropriate to take low-order moments of the TOF curve rather than to determine the velocity distribution itself, since this involves integration rather than differentiation of the TOF curve. Ratios of these moments yield quantitative information on the properties of the speed distribution (mean speed, mean energy, and speed ratio) by eliminating the unknown constant multiplier which had been dropped.

The pth moment of the speed distribution of molecules crossing a stationary reference plane is defined by

$$M_p = \int_0^\infty f(v) \, v^3 v^p \, dv. \tag{10}$$

By letting $v = \ell/\eta$, Eq. 10 can be transformed to TOF coordinates, to give

$$M_p = \int_0^\infty f(v)(\ell^{4+p}/\eta^{5+p}) \, d\eta, \tag{11}$$

where the minus sign before the integral has been dropped. Substituting for f(v)

from Eq. 9, we obtain

$$M_p = \int_0^\infty \ell^{1+p} \sum_{r=0}^\infty \frac{d}{d\eta} n(\eta - rt_{co}) \frac{1}{\eta^{1+p}} \, d\eta.$$ (12)

Integration of Eq. 12 by parts once yields

$$M_p = \ell^{1+p} \left\{ \left[\frac{1}{\eta^{1+p}} \sum_{r=0}^\infty n(\eta - rt_{co}) \right]_0^\infty + \int_0^\infty \frac{1+p}{\eta^{2+p}} \sum_{r=0}^\infty n(\eta - rt_{co}) \, d\eta \right\}.$$ (13)

The first term of Eq. 13 vanishes at both limits. Since $t_i = \eta - rt_{co}$, the integral can be rewritten

$$M_p = \int_0^\infty \left[\sum_{r=0}^\infty \frac{\ell^{1+p}(1+p)}{(t_i + rt_{co})^{2+p}} \right] n(t_i) \, dt_i,$$ (14)

where $n(t_i)$ is the height of the TOF curve at time t_i. The bracketed summation is defined as the weighting function, w_p:

$$w_p(t_i) \equiv \sum_{r=0}^\infty \frac{\ell^{1+p}(1+p)}{(t_i + rt_{co})^{2+p}}.$$ (15)

We have evaluated the weighting functions separately from the integral because the weighting functions are independent of the form of the distribution function.

The moments corresponding to $p = 0$, 1, and 2 are directly proportional to the fluxes of particles, momentum, and energy:

Particle flux $= A \, M_o$ (16a)

Momentum flux $= A \, m \, M_1 = A \, M_o \, (m \, \bar{v})$ (16b)

Energy flux $= A \, \frac{m}{2} \, M_2 = A \, M_o \left(\frac{1}{2} m \, \overline{v^2} \right),$ (16c)

where A is an unknown proportionality constant, m is the mass of the molecules, $\bar{v}$ is the mean speed $(\bar{v} \equiv M_1/M_o)$, and $\overline{v^2}$ is the mean-square speed $\left(\overline{v^2} = M_2/M_o \right)$. We shall describe our experimental results in terms of three properties defined as ratios, in order to eliminate the unknown constant A:

Mean speed: $\bar{v} = M_1/M_o$ (17a)

Mean energy: $\overline{E} = \frac{1}{2} m \overline{v^2} = \frac{1}{2} m \, M_2/M_0$ (17b)

Speed ratio: $SR = \frac{1}{\overline{v}} \left[\int_0^\infty f(v) \, v^3 (v-\overline{v})^2 \, dv \middle/ \int_0^\infty f(v) \, v^3 \, dv \right]^{1/2}$ (17c)

The speed ratio is a measure of the rms deviation of the molecular speeds from the mean speed; that is, it is a convenient parameter for expressing the width (spread) of the speed distribution. Equation 17c simplifies to

$$SR = \left[\frac{\overline{v^2}}{(\overline{v})^2} - 1 \right]^{1/2} = \left[\frac{2\overline{E}}{m(\overline{v})^2} - 1 \right]^{1/2}$$ (17d)

Because our experimental curves are to be compared with Maxwellian curves, it is necessary to derive expressions for the mean speed, mean energy, and speed ratio for the Maxwellian distribution,

$$f(v) = c \, e^{-m v^2/2kT}.$$ (18)

By substituting (18) in the previous equations, we obtain

$$\overline{v}_M = \frac{3}{4} \left(\frac{2\pi kT}{m} \right)^{1/2}$$ (19a)

$$\overline{E}_M = 2kT$$ (19b)

$$SR_M = 0.363.$$ (19c)

Equation 19 is important because it shows that the speed ratio of a Maxwellian distribution is independent of temperature and particle mass.

3. Experimental Apparatus and Procedure

The principal features of the experimental apparatus have been described previously.[5] The FET preamplifier has been modified so that it now passes higher frequency components of the signal. The preamplifier used previously shifted the TOF curve to the right because high-frequency components of the signal were attenuated. This shift made the TOF curve in the previous experiment[2] appear to agree with that corresponding to a Maxwellian distribution, but we shall see that this agreement is not observed with the improved preamplifier.

System performance runs were conducted with a heated molecular beam (1073°K),

as well as with a 300°K molecular beam. The steplike curves in Fig. III-7 are the TOF measurements, while the filled circles represent the TOF curves calculated for a Maxwellian distribution. The amplitudes of the Maxwellian curves have been normalized to fit the TOF molecular-beam curves; however, no attempt was made to force the maxima to occur at the same point on the time scale. The agreement
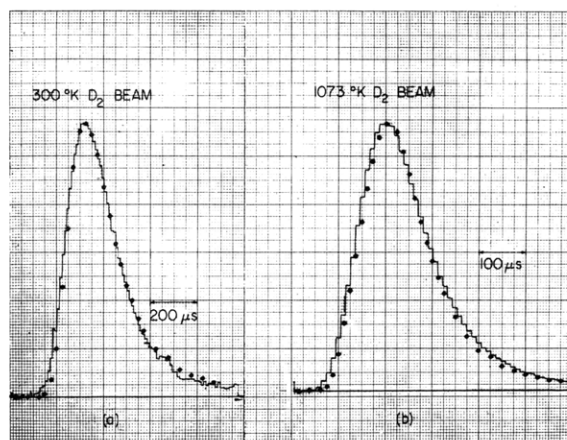

Fig. III-7. Performance test of the apparatus: (a) time-of-flight data for a D_2 molecular beam at ~300°K. (The maximum density of the beam in the detector ionizer is ~1×10^7 cm^{-3}.) (b) time-of-flight for a D_2 molecular beam at ~1073°K. In both cases, the filled circles were calculated for Maxwellian beams at the temperatures 300°K and 1073°K, respectively.

of the molecular beam and theoretical curves appears to be quite close in both cases.

The data from the system performance runs also served as a convenient test of the moment method of analysis outlined above. By applying this method to the TOF curve for T = 300°K in Fig. III-7a we obtain $\overline{E}$ = 0.050 ± 0.003 eV, which agrees satisfactorily with the corresponding value of 0.052 eV for a Maxwellian beam at 300°K. Similarly, for the curve for T = 1073°K in Fig. III-7b, we obtain $\overline{E}$ = 0.181 ± 0.015 eV, while the value for a Maxwellian beam is 0.186 eV. The speed ratios obtained for Fig. III-7a and 7b are 0.37 ± 0.01 and 0.38 ± 0.02, respectively, which agree satisfactorily with the value for a Maxwellian beam (SR$_M$ = 0.363).

4. Experimental Results

Curve A in Fig. III-8a is the TOF curve measured for the desorption of D_2 from a polycrystalline Ni membrane at 1073°K. This curve has two components: (i) molecules that permeate and desorb; (ii) molecules of the background gas in the beam chamber

that are scattered and/or desorbed from the membrane. The second component is deter-
mined by measuring the TOF curve obtained when the pressure behind the membrane
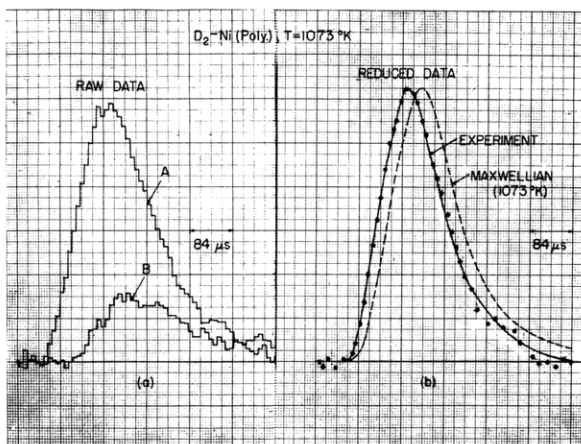is reduced until the permeation rate is negligible while the membrane temperature is

Fig. III-8.
Time-of-flight data for D_2 desorbed from
a polycrystalline Ni surface at ~1073°K.

maintained at 1073°K and the background pressure is held constant by leaking D_2 into
the chamber at a sufficient rate. The result is curve B in Fig. III-8a. Therefore, the
TOF curve for the desorbed molecules is obtained by subtracting curve B from curve A,
and this yields the curve labelled "Experiment" in Fig. III-8b. The dashed curve labelled
"Maxwellian" was computed for a Maxwellian beam at T = 1073°K. Clearly, the speed
distribution of the desorbed molecules does not correspond to that of a Maxwellian beam
at the temperature of the membrane.

The computational method described in this report has been applied to the
curve labelled "Experiment" in Fig. III-8b to determine the mean energy and
speed ratio of the desorbed molecules. This has been repeated for 10 separate
measurements of TOF curves at T = 1073°K, and the results are $\overline{E}$ = 0.27 ±
0.02 eV and SR = 0.345 ± 0.025. (The uncertainties indicate the maximum
deviations of the measurements from their averages.) Although the result for
SR does not differ significantly from that for a Maxwellian beam (SR_M = 0.363),
the result for $\overline{E}$ is ~45% greater than that for a Maxwellian beam at the tem-
perature of the sample. (According to Eq. 19b, $\overline{E}_m$ = 0.186 eV for D_2 at
1073°K.)

The mean energy and speed ratio for molecules desorbing from polycrystalline
and single-crystal (110) nickel surfaces are listed in Table III-1. The results for
T = 1173°K indicate that speed distribution is essentially the same for desorp-
tion from the single-crystal (110) surface as it is for the polycrystalline sur-
face.

Table III-1.   Comparison of experimental mean energies and speed ratios
with the corresponding Maxwellian values.

Membrane Temperature T	Maxwellian		Polycrystal Ni		(110) Single-Crystal Ni	
	$\overline{E}_M$ (eV)	SR_M	$\overline{E}$ (eV)	SR	$\overline{E}$ (eV)	SR
1073°K	0.186	0.363	0.27 ± 0.02	0.345 ± 0.025	—	—
1173°K	0.202	0.363	0.32 ± 0.02	0.389 ± 0.025	0.30 ± 0.03	0.393 ± 0.035

5. Discussion of Results

We know of only two theoretical models that provide predictions of the spatial and speed distributions of desorbed molecules.   The equilibrium model, whose development has been summarized by Loeb,[6] predicts a diffuse ($\cos \theta$) spatial distribution and a Maxwellian speed distribution.   These predictions do not agree with published experimental results.[1,7,8]   Van Willigen[7] has suggested that the activated-adsorption model of Lennard-Jones[9] may be used as a basis for developing an approximate model of the desorption of hydrogenic molecules from solid surfaces.   Expressions for the speed distribution based on the activated-adsorption model have been determined previously.[2]   We shall briefly elaborate on the activated-adsorption model and its prediction of speed distribution.

According to the activated adsorption model, the gas-solid interaction potential may be of such a nature that the atomic and molecular states of adsorption are separated by an activation energy barrier of height E_a.   For simplicity, we assume that E_a is constant over the entire surface.   By applying detail balancing, the speed distribution of the desorbed molecules is

$$f(v) = \begin{cases} 0 & \text{if } v < v^* \\ Dv^2 \exp\left(-\left(\dfrac{v}{a}\right)^2\right) & \text{if } v \geq v^* \end{cases} \tag{20}$$

where D is a constant, $a = (2kT/m)^{1/2}$, and $v^* = (2E_a/m)^{1/2}$.   This means that the desorbed molecules will have energies greater than E_a and, therefore, velocities greater than v^*.   Now we have to transform this distribution to time-of-flight coordinates in order to be able to compare it with the experimental measurements. The dimensionless form of the TOF distribution becomes[2]

$$\bar{n}_N(\bar{t}_i) = \frac{1}{\bar{t}_{co}} \left\{ \frac{1}{\bar{t}^O} e^{-\frac{1}{\bar{t}^{O^2}}} - \frac{1}{\bar{t}_i - \bar{t}^*} e^{\left[-\frac{1}{\left(\bar{t}_i - \bar{t}^*\right)^2} \right]} \right.$$

$$\left. + \frac{\sqrt{\pi}}{2} \left[\mathrm{erf}\left[\frac{1}{\bar{t}_i - \bar{t}^*} \right] - \mathrm{erf}\left(\frac{1}{\bar{t}^O} \right) \right] \right\}, \tag{21}$$

where $\bar{t}^O \equiv (kT/E_a)^{1/2}$, with T the temperature of the surface, $t^* = t_i$ for $t_i < t_{co}$, and $t^* = t_{co}$ for $t_i > t_{co}$.

For the spatial distributions of Dabiri,[1] we find that a reasonably good fit is obtained when $E_a \sim 0.20$ eV. The speed distribution calculated for $E_a = 0.20$ eV at $T = 1073°$K is plotted in Fig. III-9, together with the experimental TOF curve for polycrystalline Ni
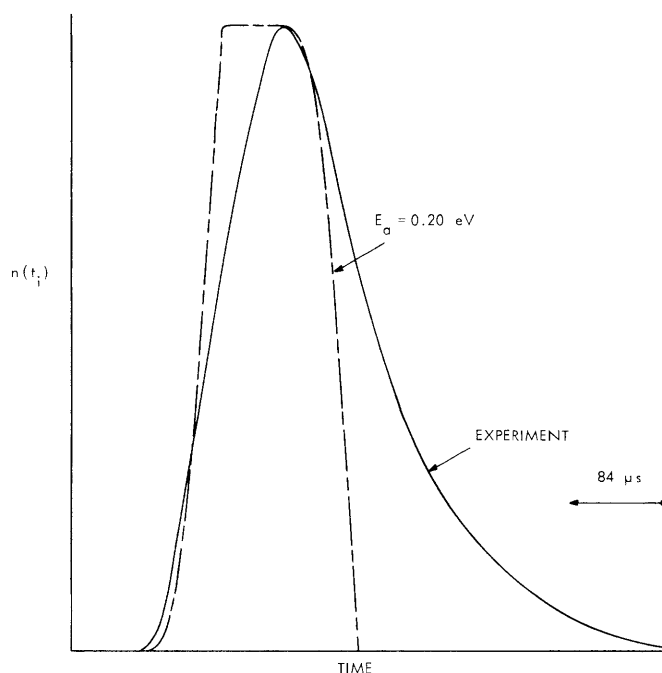

Fig. III-9.   Comparison of experimental TOF curve for D_2 desorbed from a Ni surface at ~1073°K (solid curve) with the TOF curve predicted by the activated adsorption model for $E_a = 0.20$ eV (dashed curve).

at $T = 1073°$K. The van Willigen model does not appear to be able to predict the shape of the TOF curve of the desorbed molecules.

By using the moment method outlined in this report, the mean energy and speed ratio

were calculated for the TOF curve predicted by the van Willigen model. For $E_a = 0.20$ eV and T = 1073°K, $\overline{E}$ = 0.322 eV and SR = 0.164. These values deviate markedly from the experimental curve ($\overline{E}$ = 0.27 ± 0.02 eV and SR = 0.345 ± 0.025).

<div align="right">T. E. Kenney, A. E. Dabiri, R. E. Stickney</div>

References

1. A. E. Dabiri and R. E. Stickney, Quarterly Progress Report No. 97, Research Laboratory of Electronics, M. I. T. , April 15, 1970, p. 17.

2. A. E. Dabiri and R. E. Stickney, Quarterly Progress Report No. 99, Research Laboratory of Electronics, M. I. T. , October 15, 1970, p. 47.

3. J. P. Moran, Report No. 68-1, Fluid Dynamics Research Laboratory, M. I. T. , February, 1968.

4. F. B. Hildebrand, Advanced Calculus for Engineers (Prentice-Hall, Inc. , Englewood Cliffs, N. J. , 1962), pp. 74-77.

5. A. E. Dabiri and R. E. Stickney, Quarterly Progress Report No. 95, Research Laboratory of Electronics, M. I. T. , October 15, 1969, p. 19.

6. For a review of the literature pertaining to this problem, see L. B. Loeb, Kinetic Theory of Gases (McGraw-Hill Book Company, New York, 2d edition, 1934).

7. W. van Willigen, Phys. Letters 28A, 80 (1968).

8. R. L. Palmer, J. N. Smith, H. Saltsburg, and D. R. O'Keefe, J. Chem. Phys. 53, 1666 (1970).

9. J. E. Lennard-Jones, Trans. Faraday Soc. 28, 333 (1932).